Electronic structure of the thermoelectric materials Bi_2Te_3 and Sb_2Te_3 from first-principles calculations

Guofeng Wang[*] and Tahir Cagin[†]

Department of Chemical Engineering, Texas A&M University, College Station, Texas 77840, USA
(Received 15 February 2007; revised manuscript received 2 May 2007; published 1 August 2007)

The electronic structures of Bi_2Te_3 and Sb_2Te_3 crystals were calculated using the first-principles full-potential linearized augmented plane-wave method. We studied not only the unrelaxed crystals, which have the experimental lattice parameters and scaled atom coordinates, but also the relaxed crystals, which have the lattice parameters and scaled atom coordinates determined from theoretical structure optimizations. We found that Bi_2Te_3 has six highest valence-band edges and six lowest conduction-band edges regardless of relaxations. However, by varying structural parameters Sb_2Te_3 may undergo an electronic topological transition that the number of valence (and conduction) band edges changes between 6 and 12. Moreover, we presented the location of the band edges and the effective mass tenor parameters for electrons and holes associated with those band edges. Furthermore, we discussed the relation of the calculated electronic structures of the two crystals with the electrical properties of Bi_2Te_3/Sb_2Te_3 superlattices.

I. INTRODUCTION

High-performance thermoelectric materials have great impact to our society owing to their applications in cooling and power generation.[1,2] The performance of thermoelectric materials is described by the figure of merit (ZT),

$$ZT = S^2\sigma T/(\kappa_e + \kappa_L), \tag{1}$$

where S is the Seebeck coefficient, σ is the electrical conductivity, T is the temperature of the sample, and κ_e and κ_L are the thermal conductivities due to the electron and lattice, respectively. A higher value of ZT indicates a better thermoelectric performance for the given material. From the definition of ZT [Eq. (1)], it is seen that increasing electrical conductivity and/or decreasing thermal conductivity are constructive in enhancing the thermoelectric performance of materials. Thus, it was suggested that "phonon-glass electron crystal" (PGEC), which has the thermal properties of a glass and the electronic properties of a crystal, would be the best thermoelectric material.[3] This PGEC approach to developing thermoelectric materials has been employed in the thermoelectric research work of clathrates,[4,5] skutterudites,[6,7] and disordered[8] and nanostructured[9,10] materials.

To date, p-type Bi_2Te_3/Sb_2Te_3 superlattices have been found to have the highest ZT of about 2.4 at 300 K.[9] The periodic superlattices were grown along their c axis, in which Bi_2Te_3 and Sb_2Te_3 are layered with a weak van der Waals-like bonding.[11] The observed excellent thermoelectric performance is believed to be caused by the phonon-blocking and/or electron-transmitting behavior of the superlattices in their cross-plane direction (c axis). The phonon-blocking effect in the Bi_2Te_3/Sb_2Te_3 superlattices has been systematically examined. It was found that κ_L of the superlattices could be more than two times lower than that of a solid solution alloy, depending on the period of the superlattice.[12] The reduction of thermal conductivity in superlattices can be explained by assuming that phonon transport at the interface is partially diffuse and partially specular, and that inelastic phonon scattering happens at the

interface.[13] For the electron-transmitting effect in the Bi_2Te_3/Sb_2Te_3 superlattices, experimental measurements show that the electron cross-plane mobility increases with the increase of the Sb_2Te_3 content in the superlattices.[9] In a previous letter,[14] we provided an explanation to that behavior of the Bi_2Te_3/Sb_2Te_3 superlattices based on the first-principles calculation of the effective masses of Bi_2Te_3 and Sb_2Te_3 crystals. In this paper, we present the detailed electronic structure calculations for both unrelaxed and relaxed Bi_2Te_3 and Sb_2Te_3 crystals using first-principles methods.

First-principles methods, without any parametrization to experimental results, have been developed and applied to investigating and searching those promising candidates of thermoelectric materials.[15–17] Particularly, accurate electronic structures of thermoelectric crystals are readily attainable through first-principles calculations. Electronic structure calculations are very important in determining if a material is suitable for thermoelectric applications. This is because the ZT of thermoelectric materials depends on band structures such as the band gap, effective mass and its anisotropy, degeneracy of the band extremes, and carrier mobility. First-principles electronic structure calculations have already been conducted for the Bi_2Te_3 (Refs. 15 and 18–21) and Sb_2Te_3 (Refs. 14 and 22) crystals with the experimental lattice parameters. Distinct from those previous works, we compute the electronic structures for Bi_2Te_3 and Sb_2Te_3 with fully relaxed crystal structures in this work. Some features in the electronic structures emerge after we relax the crystal structures. For Sb_2Te_3, we found 12 conduction-band valleys and 12 valence-band valleys for the relaxed crystal, while we found only 6 conduction-band valleys and 6 valence-band valleys for the unrelaxed crystal. The calculated electronic structures in this work are useful to qualitatively estimate the thermoelectric figure of merit of the materials.[23] Moreover, the calculated band structure and effective mass tensor can be used to inform parametrized tight-binding models, which are both atomistic and efficient to perform large scale device simulations.[24]
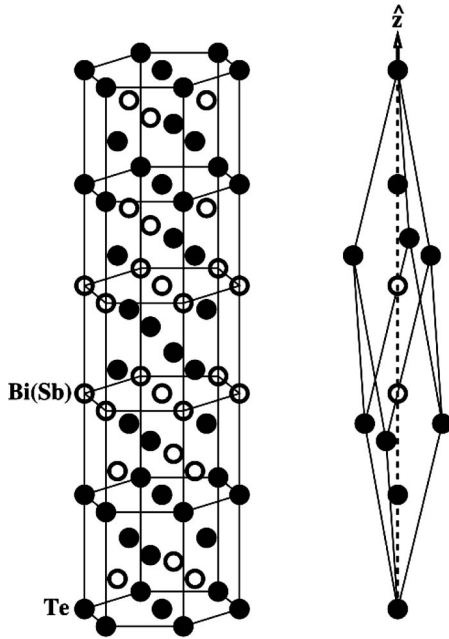
FIG. 1. Crystal structure of Bi_2Te_3 and Sb_2Te_3: (left) hexagonal cell and (right) rhombohedral cell. In the figure, the open cycles represent Bi (or Sb) atoms and the dark cycles represent Te atoms.

II. CALCULATION METHOD

We performed electronic structure calculations using the self-consistent full-potential linearized augmented plane-wave (FPLAPW)[25] method within density functional theory (DFT) and the generalized gradient approximation (GGA) of Perdew *et al.* for the exchange and correlation potential,[26] as implemented in the FLEUR code.[27] Spin-orbit interaction, which is essential for calculating the electronic structure of Bi_2Te_3 and Sb_2Te_3,[15,18–22] has been included in our calculations. We used 60 k points for the k-space integration, which is sufficient for an electronic structure calculation of semiconductors.[20] We set the energy cutoff between the core and valence states at -1.8 Ry. In this way, there are 48 valence electrons in a rhombohedral Bi_2Te_3 (or Sb_2Te_3) unit cell. For crystal structure relaxation, we alternatively relaxed the lattice parameters and atomic internal coordinates until an energy minimum is achieved. The fully relaxed structures are ensured by checking both the energy and the force: the energies of two subsequent iterations do not differ by more than 10^{-4} hartree and the forces of two subsequent iterations do not differ by more than 10^{-5} hartree/a.u.

III. RESULTS

A. Crystal structures

Bulk Bi_2Te_3 (or Sb_2Te_3) has a rhombohedral crystal structure which is with the space group D_{3d}^5 ($R\bar{3}m$) and with five atoms in a unit cell. A rhombohedral structure can be visualized as a layer structure and a hexagonal lattice cell. We plot this hexagonal cell in the left panel of Fig. 1. In the hexagonal cell of Bi_2Te_3 (or Sb_2Te_3), there are five individual atomic layers in the sequence of Te-Bi(Sb)-Te-
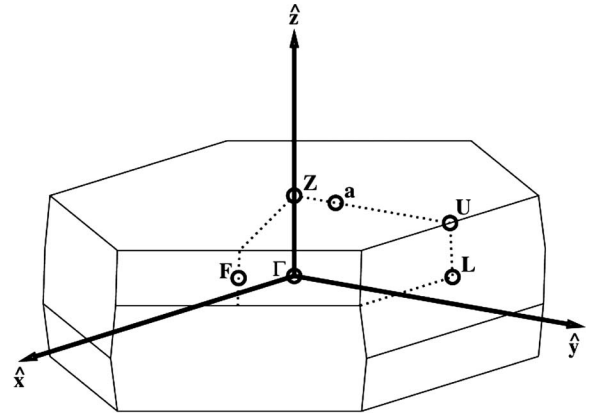
FIG. 2. Brillouin zone of Bi_2Te_3 and Sb_2Te_3 crystals. In the figure, the binary axis (with twofold rotation symmetry) is along x, the bisectrix axis (in the reflection plane) is along y, and the trigonal axis (with threefold rotation symmetry) is along z. The high-symmetry k points are marked in the figure using open circles.

Bi(Sb)-Te along the trigonal axis. In the right panel of Fig. 1, we plot the rhombohedral unit cell which was adopted in our calculations. The corresponding Brillouin zone for the two crystals is given in Fig. 2.

In Table I, we give the lattice parameters and scaled atom coordinates for Bi_2Te_3 and Sb_2Te_3 from experimental measurements.[28] We assumed those values in our calculations of unrelaxed crystals. We also give in Table I the theoretical lattice parameters and scaled atom coordinates obtained from first-principles relaxation calculations. Our theoretical results for Bi_2Te_3 differ from experimental data by 3.3% for lattice constant a, 0.5% for lattice constant c, 1.4% for the scaled coordinate of Te atoms, and 0.0% for the scaled coordinate of Bi atoms. Our theoretical results for Sb_2Te_3 differ from experimental data by 4.5% for lattice constant a, 0.4% for lattice constant c, 0.9% for the scaled coordinate of Te atoms, and 0.0% for the scaled coordinate of Sb atoms. Thus, our calculated theoretical crystal structures are very close to the experimental ones. In this work, we also

TABLE I. Comparison of the theoretically optimized with experimentally measured lattice parameters of Bi_2Te_3 and Sb_2Te_3 crystals. In the table, a and c are the lattice parameters in the hexagonal lattice (see the left panel of Fig. 1); $\mu(\text{Te})$, $\mu(\text{Bi})$, and $\mu(\text{Sb})$ are the scaled coordinates of the Te, Bi, and Sb atoms, which are inside the unit cell (see the right panel of Fig. 1), along the trigonal axis (z) of the crystals.

	Bi_2Te_3		Sb_2Te_3	
	Theory	Expt.[a]	Theory	Expt.[a]
a (Å)	4.53	4.3835	4.44	4.25
c (Å)	30.63	30.487	30.29	30.4
$\mu(\text{Te})$	±0.209	±0.212	±0.209	±0.211
$\mu(\text{Bi})$ or $\mu(\text{Sb})$	±0.400	±0.400	±0.400	±0.400

[a]Reference 28.
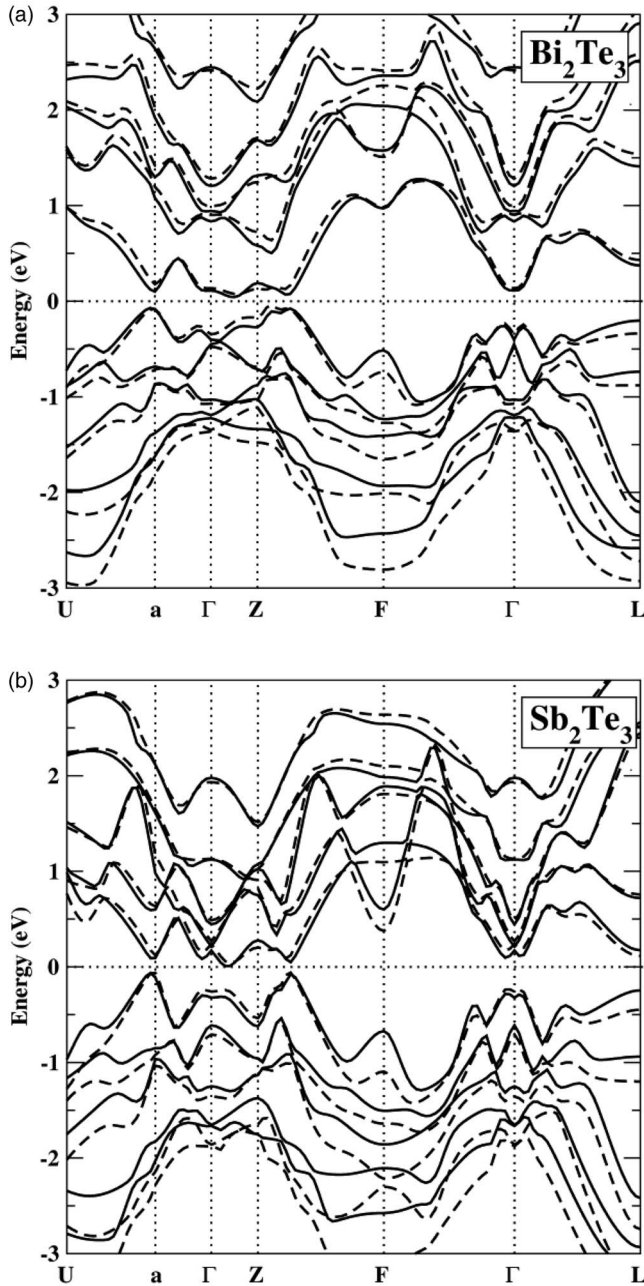
FIG. 3. Electronic band structure of (a) Bi_2Te_3 and (b) Sb_2Te_3 along the high-symmetry lines from FLAPW calculations and with spin-orbit interaction. The solid lines show the calculation results for the crystals with the optimized lattice parameters, while the dashed lines give the results for the crystals with the experimental lattice parameters.

performed electronic structure calculations for relaxed Bi_2Te_3 and Sb_2Te_3 crystals using these theoretical values.

B. Electronic structures

The band structures of both the relaxed and unrelaxed Bi_2Te_3 and Sb_2Te_3 crystals were evaluated along some high-symmetry lines and plotted in Fig. 3. The locations of those high-symmetry k points are marked in the Brillouin zone of

Fig. 2. For both Bi_2Te_3 and Sb_2Te_3, we found in Fig. 3 two valence-band maxima, along Γa and ZF directions, respectively, and three conduction-band minima, along Γa, ZF, and ΓZ directions, respectively. Shown in Fig. 2, high-symmetry k points Γ, a, Z, and F all lie in the plane (denoted as yz plane) containing the bisectric (y) axis and the trigonal (z) axis. Hence, our results in Fig. 3 indicate that the highest valence-band edge (VBE) and lowest conduction-band edge (CBE) of Bi_2Te_3 and Sb_2Te_3 lie in that plane. Here, we found similar results as those from previous first-principles calculations.[18–22] In addition, Fig. 3 shows that the calculated electronic structures do not differ much between the relaxed and unrelaxed Bi_2Te_3 and Sb_2Te_3 crystals along those high-symmetry lines.

To find the exact locations of VBE and CBE for Bi_2Te_3 and Sb_2Te_3, we have sampled the eigenvalues of 525 k points homogeneously distributed in the yz plane within the irreducible Brillouin zone. The VBE and CBE were searched among those extremes of the eigenvalues. Further, we ensured the found VBE and CBE to be the real band edges by evaluating E vs k along various orthogonal directions around those k points. We found that all VBE and CBE of Bi_2Te_3 and Sb_2Te_3 are within the yz plane but off the high-symmetry lines.

Since all calculated extremes in the electronic bands of Bi_2Te_3 and Sb_2Te_3 lie in the yz plane, the energy near their VBE and CBE can be expressed as[19]

$$\frac{2m_e E}{\hbar^2} = \alpha_{xx}k_x^2 + \alpha_{yy}k_y^2 + \alpha_{zz}k_z^2 + 2\alpha_{yz}k_y k_z, \qquad (2)$$

where m_e is the free-electron mass, E is the energy relative to the energy of VBE or CBE, and α_{ij} is the component of effective mass tensor. We can calculate the effective tensor α_{ij} by fitting the calculated E vs k to parabolas along various orthogonal directions (x, y, z, and yz). In this work, we varied k_x, k_y, and k_z between -0.005 and 0.005 Å^{-1} around the VBE and CBE of the Bi_2Te_3 and Sb_2Te_3 crystals.

Below, we present our findings in detail.

1. Bi₂Te₃

Figure 4(a) shows the locations of VBE for the relaxed Bi_2Te_3 using the contour plot of the highest valence band in the yz plane of the Brillouin zone. We found two band edges, which are marked as VBE and X in the figure. VBE is about 27 meV higher than X and thus is our predicted VBE for the relaxed Bi_2Te_3. Figure 4(a) also shows that VBE is more isotropic in the yz plane than X. It is noted that band edge X was predicted to be the highest valence-band edge from previous first-principles calculations with local density approximation (LDA) for the exchange and correlation potential.[20,21] In contrast to their results, our current results of VBE and X are in agreement with those from a previous GGA-DFT calculation.[15] It appears that the difference between LDA and GGA leads to the discrepancy in the predicated location of VBE. In Fig. 4(b), we found one CBE for the relaxed Bi_2Te_3. Figures 4(c) and 4(d) show the energy contour plots for the unrelaxed Bi_2Te_3 crystal. In those figures, we located one VBE and one CBE.
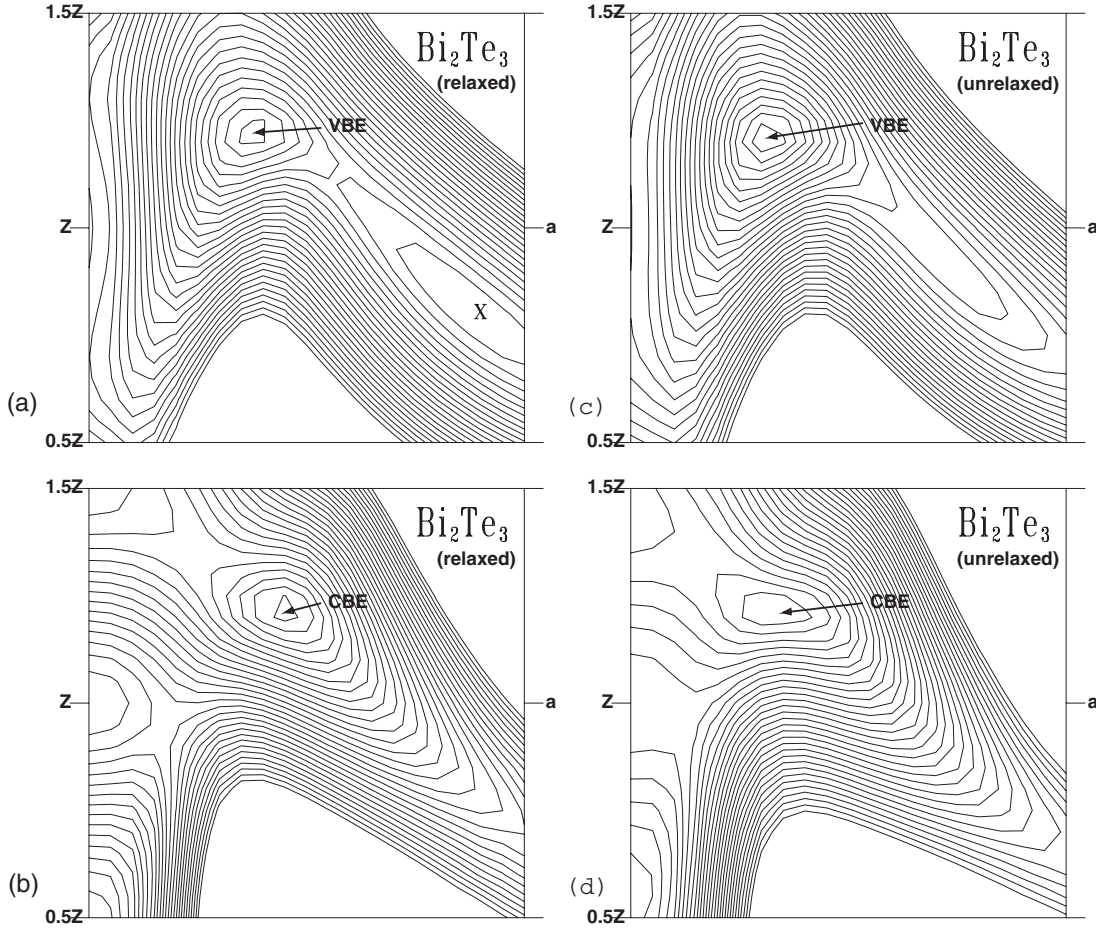
FIG. 4. Contour plots of the eigenvalues of (a) the highest valence band of relaxed Bi_2Te_3, (b) the lowest conduction band of relaxed Bi_2Te_3, (c) the highest valence band of unrelaxed Bi_2Te_3, and (d) the lowest conduction band of unrelaxed Bi_2Te_3 in the yz plane, where $Z=[0.5,0.5,0.5]$ and $a=[0.64,0.43,0.43]$ in the basis vectors of the reciprocal lattice. In the figures, the locations of VBE and CBE are marked. In (a), symbol X marks the location of VBE found in previous LDA calculations (Refs. [20] and [21]). In the plots, the energy difference is 10 meV between two neighboring lines.

We give in Table II the locations of the found band edges of Bi_2Te_3 in the reciprocal lattice. It is found that, for both relaxed and unrelaxed Bi_2Te_3, the VBE and CBE lie inside the yz plane of the Brillouin zone. Owing to the high-symmetry of the yz plane, there would be a total of 6 degen-

TABLE II. Location of the valence-band edge (VBE) and conduction-band edge (CBE) of Bi_2Te_3 (shown in Fig. 4) given by the basis vectors of the reciprocal lattice.

Band edges	Locations
Relaxed Bi_2Te_3	
VBE	[0.662,0.584,0.584]
X[a]	[0.531,0.348,0.348]
CBE	[0.673,0.579,0.579]
Unrelaxed Bi_2Te_3	
VBE	[0.650,0.584,0.584]
CBE	[0.652,0.585,0.585]

[a]Band edge X is 26.7 meV lower than VBE in the highest valence band.

erated VBEs and CBEs in the Brillouin zone of Bi_2Te_3. Our theoretical results about the location and number of VBEs and CBEs agree well with previous experimental measurements.[29,30]

Moreover, the calculated effective mass tensor for the holes at VBE and for the electrons at CBE are given in Table III for both relaxed and unrelaxed Bi_2Te_3. First of all, our results agree satisfactorily with the experimental data[29,30] and previous LDA results.[21] Compared to those for unrelaxed Bi_2Te_3, the calculated effective mass parameters for relaxed Bi_2Te_3 (especially, for the electrons at CBE) are in better agreement with experiments. However, the improvement is not significant.

2. Sb_2Te_3

For relaxed Sb_2Te_3, we found in Figs. 5(a) and 5(b) two valence-band edges (VBE1 and VBE2) and two conduction-band edges (CBE1 and CBE2) in the yz plane of the Brillouin zone. VBE1 and VBE2 differ in energy by 4.9 meV; CBE1 and CBE2 differ in energy by 1.6 meV. Since the energy difference is very small, we count both of them as Fermi surface pockets. Interestingly, we found in Figs. 5(c)

TABLE III. Theoretical and experimental values of effective mass tensor parameters (in unit of m_e^{-1}, m_e is free-electron mass) for the holes associated with the valence-band edge and for the electrons associated with the conduction-band edge of Bi_2Te_3. The angle $\theta_{yz} = \frac{1}{2}\arctan[2\alpha_{yz}/(\alpha_{zz}-\alpha_{yy})]$ is the principal angle of the energy ellipsoid in the yz plane with respect to the bisectrix y axis.

Valence band	This work			sX-LDA[a]	Expt.[b]
	VBE (relaxed)	X (relaxed)	VBE (unrelaxed)		
α_{xx}	30.2	34.6	30.6	39.5	32.5
α_{yy}	6.8	3.7	10.6	3.8	4.81
α_{zz}	10.9	5.7	13.8	5.2	9.02
α_{yz}	0.8	4.2	1.1	6.2	4.15
θ_{yz}	10.6°	38.3°	17.4°	41°	31.5°
Conduction band	This work			sX-LDA[a]	Expt.[c]
	CBE (relaxed)		CBE (unrelaxed)		
α_{xx}	44.0		34.7	52.2	46.9
α_{yy}	7.2		3.9	8.0	5.92
α_{zz}	12.5		13.3	7.3	9.50
α_{yz}	3.7		2.8	3.8	4.22
θ_{yz}	27.2°		15.5°	−42.4°	33.5°

[a]Reference 21.
[b]Reference 29.
[c]Reference 30.

and 5(d) for unrelaxed Sb_2Te_3 only one VBE and one CBE in the yz plane of the Brillouin zone. VBE of the unrelaxed Sb_2Te_3 corresponds to VBE1 of the relaxed Sb_2Te_3, while CBE of the unrelaxed Sb_2Te_3 corresponds to CBE2 of the relaxed Sb_2Te_3. Our calculations show that VBE2 and CBE1 are not stable band edges anymore for the unrelaxed Sb_2Te_3. Therefore, we predicted a 12-band model (12 valence valleys and 12 conduction valleys) for the relaxed Sb_2Te_3 but a 6-band model (6 valence valleys and 6 conduction valleys) for the unrelaxed Sb_2Te_3. We used identical parameters in the two calculations. The only difference between the two calculations is the slight variation in lattice parameters and scaled atom coordinates given in Table I. For both relaxed and unrelaxed Sb_2Te_3, Table IV lists the locations of those band edges and Table V gives the calculated effective mass tensor parameters at those band edges.

It appears that experimental measurements of the electronic structure of Sb_2Te_3 also yielded conflicting results. Schwartz *et al.* measured the Fermi surface of p-type Sb_2Te_3 by the de Hass–van Alphen effect and found six valence-band ellipsoids.[31] In contrast, von Middendorff claimed that their data from the Shubnikov–de Hass effect in p-type Sb_2Te_3 crystals supported a 12 valence band model.[32] Moreover, it was reported that for alloy $Sb_{1.5}Bi_{0.5}Te_3$, the value of ZT increases by at least a factor of 2 at about 2 GPa pressure from its value at ambient pressure.[33] To explain that observation, electronic topological transition (Fermi surface topology change under compression) for $Sb_{1.5}Bi_{0.5}Te_3$ under pressure was suggested.[34] Those previous works make us believe that our first-principles results for the band edge degeneracy (12 for the relaxed Sb_2Te_3 and 6 for the unrelaxed Sb_2Te_3) are reasonable and manifesting a possible electronic topological transition under the influence of lattice parameters and atomic positions for alloy Sb_2Te_3. Recently, Larson systematically examined the effect of uniaxial stresses on the electronic structures of Sb_2Te_3 crystals and also found the changes in the valence-band maximum (from 6 to 12) for Sb_2Te_3.[35] In Ref. 35, Larson used a full-potential linear muffin tin orbital method within the local spin density approximation. In this work, we used the FPLAPW-GGA method. Both of the two independent first-principles calculations predict a Fermi surface topology change in Sb_2Te_3 crystals when changing lattice parameters, so it is worthwhile to further experimentally investigate this phenomenon.

C. Band gaps

Band gap is an important parameter when designing high-performance thermoelectric materials. The analysis in Ref. 23 points out that the thermoelectric semiconductors must have a band gap of at least $10k_BT$ (k_B is Boltzmann constant and T is the maximum operating temperature) in order to have an optimum thermoelectric performance. Unfortunately, DFT most often does not predict the band gap accurately. Our current calculations suffer the same problems. We calculated the band gaps for the relaxed and unrelaxed Bi_2Te_3 and Sb_2Te_3 crystals by evaluating the energy difference between the lowest CBE and the highest VBE. Our results are
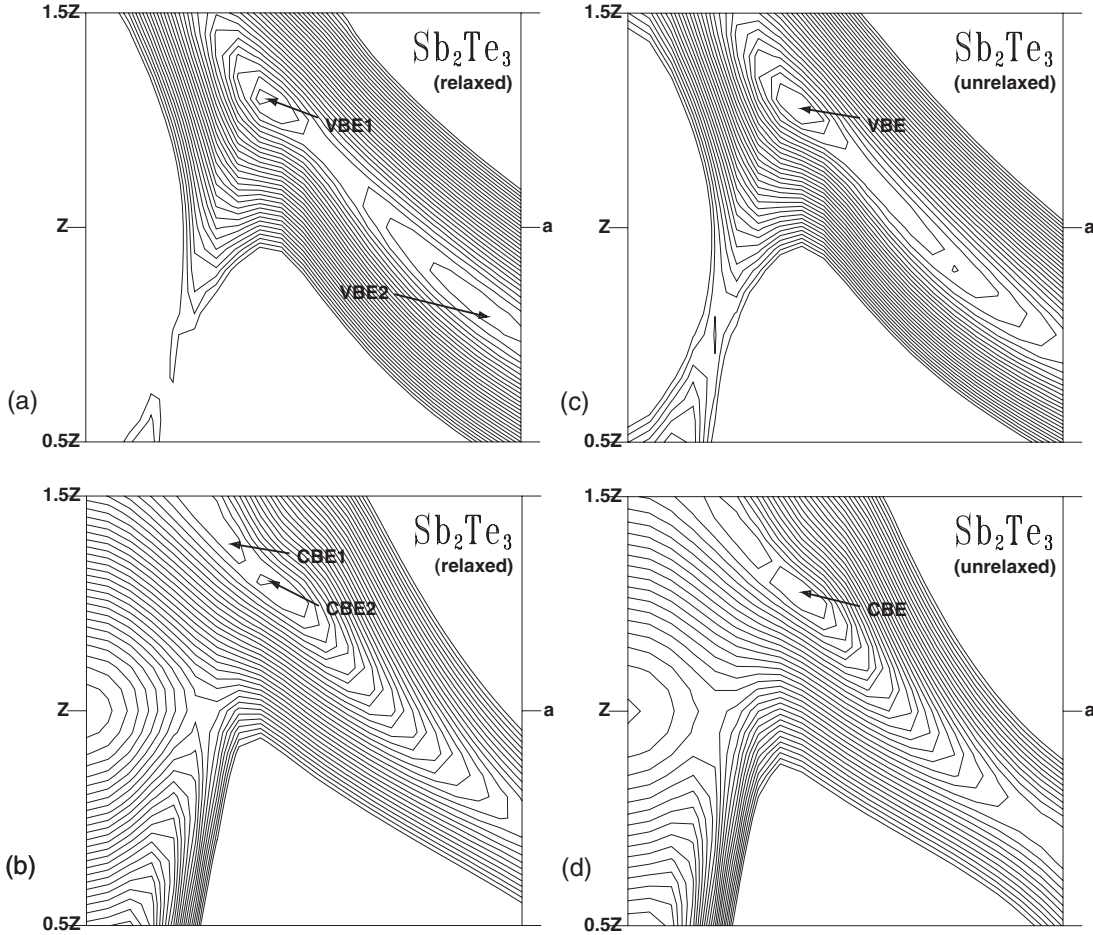
FIG. 5. Contour plots of the eigenvalues of (a) the highest valence band of relaxed Sb_2Te_3, (b) the lowest conduction band of relaxed Sb_2Te_3, (c) the highest valence band of unrelaxed Sb_2Te_3, and (d) the lowest conduction band of unrelaxed Sb_2Te_3 in the yz plane, where $Z=[0.5,0.5,0.5]$ and $a=[0.64,0.43,0.43]$ in the basis vectors of the reciprocal lattice. In the figures, the locations of VBEs and CBEs are marked. In the plots, the energy difference is 10 meV between two neighboring lines.

given in Table VI. Compared to experimental values,[36] our predicted band gaps are significantly lower. We observe a slight improvement in the agreement between theory and ex-

TABLE IV. Location of the valence-band edge (VBE) and conduction-band edge (CBE) of Sb_2Te_3 (shown in Fig. 5) given by the basis vectors of the reciprocal lattice.

Band edges	Locations
	Relaxed Sb_2Te_3
VBE1	[0.705,0.615,0.615]
VBE2[a]	[0.534,0.341,0.341]
CBE1	[0.790,0.737,0.737]
CBE2[b]	[0.703,0.612,0.612]
	Unrelaxed Sb_2Te_3
VBE	[0.695,0.613,0.613]
CBE	[0.690,0.605,0.605]

[a]VBE2 is 4.9 meV lower than VBE1 in the highest valence band.
[b]CBE2 is 1.6 meV higher than CBE1 in the lowest conduction band.

periment if we fully relax the crystals. However, the improvement is not pronounced.

IV. DISCUSSIONS AND CONCLUSIONS

In this work, we calculated the electronic structure of Bi_2Te_3 and Sb_2Te_3 crystals using first-principles method. We conducted our study for both the unrelaxed (with the experimental lattice parameters and scaled atom coordinates) and relaxed (with the lattice parameters and scaled atom coordinates from theoretical optimization) crystals.

We found six valence- and six conduction-band edges in the trigonal-bisectrix (yz) plane of the Brillouin zone for both relaxed and unrelaxed Bi_2Te_3. Our theoretical results are consistent with experimental measurements.[29,30] Although the structural difference (lattice parameters and scaled atom coordinates) between the relaxed and unrelaxed Sb_2Te_3 crystals is quite small (see Table I), we witnessed a dramatic change in the topology of their Fermi surfaces. The relaxed Sb_2Te_3 crystal has 12 valence- and 12 conduction-band edges in the trigonal-bisectrix (yz) plane of the Brillouin zone, while the unrelaxed one has only 6 valence- and

TABLE V. Theoretical values of effective mass tensor parameters (in unit of m_e^{-1}, m_e is free-electron mass) for the holes associated with the valence-band edge and the electrons associated with the conduction-band edge of Sb_2Te_3. The angle $\theta_{yz} = \frac{1}{2} \arctan[2\alpha_{yz}/(\alpha_{zz} - \alpha_{yy})]$ is the principal angle of the energy ellipsoid in the yz plane with respect to the bisectrix y axis.

	Relaxed				Unrelaxed	
	VBE1	VBE2	CBE1	CBE2	VBE	CBE
α_{xx}	46.6	36.5	37.1	46.6	45.1	42.7
α_{yy}	17.6	6.6	9.2	11.9	18.2	14.5
α_{zz}	20.6	12.6	5.9	18.6	22.1	20.9
α_{yz}	13.3	8.6	6.6	13.1	14.1	13.9
θ_{yz}	41.8°	35.6°	−37.9°	37.8°	41.1°	38.4°

6 conduction-band edges in the same yz plane. It appears that the degeneracy of band edges in Sb_2Te_3 is sensitively influenced by the changes in its crystal structural parameters. Analysis in Ref. 23 suggests that ZT is a monotonically increasing function of the degeneracy of band edges of thermoelectric materials. Hence, our results for the topological change in the Fermi surface of Sb_2Te_3 might be the explanation to the observations of a sharp increase in ZT by a factor of 2 in the compressed Sb-riched $Sb_{1.5}Bi_{0.5}Te_3$ alloys.[33]

Tables II and IV show that both Bi_2Te_3 and Sb_2Te_3 have VBEs and CBEs in the same yz plane of the Brillouin zone and the VBEs and CBEs of the two crystals (VBE1 and CBE2 for the relaxed Sb_2Te_3) are very close in k space. Therefore, the band edge degeneracy (six) of bulk Bi_2Te_3 and Sb_2Te_3 could be well preserved in the Bi_2Te_3/Sb_2Te_3 superlattices. This is helpful for the superlattices to behave like a pure crystal in conducting electrons and holes through its interfaces between different Bi_2Te_3 and Sb_2Te_3 layers. High band edge degeneracy would lead to high carrier density and hence larger electrical conductivity.

The Bi_2Te_3/Sb_2Te_3 superlattices were grown along the trigonal (z) axis,[11] so the carrier (electron or hole) mobility in the two crystals along the z axis would determine the mobility of the carriers across the superlattice interfaces. In the theory of transport in semiconductors, the carrier is treated as a classical particle with momentum and effective mass.[37] The smaller the effective mass, the higher the mobility of carriers. Within the envelope function approximation and when the offset potential is small, the effective mass for carrier motion parallel to the growth direction of the superlattices is written as[38]

$$m_S = \frac{L_1}{L_1 + L_2} m_1 + \frac{L_2}{L_1 + L_2} m_2, \tag{3}$$

where m_S, m_1, and m_2 are the effective masses along the superlattice growth direction for the superlattice and its two component semiconductors, respectively. L_1 and L_2 are the layer thicknesses of the two components.

Effective mass m is equal to $1/\alpha$. For Bi_2Te_3 and Sb_2Te_3 crystals, the values of α are given in Tables III and V. Our results indicate that the same carrier would have a less effective mass m_{zz} (a larger α_{zz}) along the z axis in Sb_2Te_3 than in Bi_2Te_3. Here, we only include VBE1 (and CBE2) of the relaxed Sb_2Te_3 into comparisons since they are closer to VBE (and CBE) of Bi_2Te_3 than VBE2 (and CBE1) and hence contribute more significantly in conducting carriers in the Bi_2Te_3/Sb_2Te_3 superlattices. Considering Eq. (3), the effective mass m_{zz} of the carriers in the Bi_2Te_3/Sb_2Te_3 superlattices will be reduced if there are more Sb_2Te_3 than Bi_2Te_3 in each period. In other words, the mobility of carriers in the cross-plane (z) direction would increase with more Sb_2Te_3 component in the superlattice, agreeing excellently with the experimental results given in Fig. 2(c) of Ref. 9. In an early work, Mahanti *et al.* calculated the electronic structure of $(Bi_2Te_3)_m(Sb_2Te_3)_n$ superlattices directly using first-principles method.[39] Although they did not fully relax the internal structures in their calculations, their results still showed a clear reduction of the effective mass m_{zz} in the superlattices compared to the corresponding value of Bi_2Te_3. That agrees with our above prediction for Bi_2Te_3/Sb_2Te_3 superlattices.

In conclusion, the electronic structures of the thermoelectric crystals can be accurately obtained from first-principles

TABLE VI. Theoretical and experimental values of band gap (in unit of meV) for Bi_2Te_3 and Sb_2Te_3.

	Bi_2Te_3			Sb_2Te_3		
	Relaxed	Unrelaxed	Expt.[a]	Relaxed	Unrelaxed	Expt.[a]
Band gap	49	26	130	30	22	280

[a]Reference 36.

calculations. The main features of the theoretical electronic structure of Bi_2Te_3 and Sb_2Te_3 are consistent with experimental data. Furthermore, the electron-transmitting behavior across the interfaces of the Bi_2Te_3/Sb_2Te_3 superlattices can be explained using the electronic structures of their component crystals. Therefore, the first-principles electronic structure calculations are very useful for designing semiconductor superlattices with high thermoelectric performance.

*Present address: Department of Chemistry and Physics, University of South Carolina Aiken, Aiken, SC 29801; guofengw@usca.edu

†Corresponding author; tahir.cagin@chemail.tamu.edu

[1] F. J. DiSalvo, Science **285**, 703 (1999).

[2] G. Chen, M. S. Dresselhaus, G. Dresselhaus, J. P. Fleurial, and T. Caillat, Int. Mater. Rev. **48**, 45 (2003).

[3] G. A. Slack, in *CRC Handbook of Thermoelectrics*, edited by D. M. Rowe (CRC, Boca Raton, FL, 1995), pp. 407–440.

[4] C. S. Nolas, J. L. Cohn, G. A. Slack, and S. B. Schujman, Appl. Phys. Lett. **73**, 178 (1998).

[5] A. Bentien, M. Christensen, J. D. Bryan, A. Sanchez, S. Paschen, F. Steglich, G. D. Stucky, and B. B. Iversen, Phys. Rev. B **69**, 045107 (2004).

[6] B. C. Sales, D. Mandrus, and R. K. Williams, Science **272**, 1325 (1996).

[7] G. S. Nolas, D. T. Morelli, and T. M. Tritt, Annu. Rev. Mater. Sci. **29**, 89 (1999).

[8] G. J. Snyder, M. Christensen, E. Nishibori, T. Caillat, and B. B. Iversen, Nat. Mater. **3**, 458 (2004).

[9] R. Venkatasubramanian, E. Siivola, T. Colpitts, and B. O'Quinn, Nature (London) **413**, 597 (2001).

[10] T. C. Harman, P. J. Taylor, M. P. Walsh, and B. E. LaForge, Science **297**, 2229 (2002).

[11] R. Venkatasubramanian, T. Colpitts, B. O'Quinn, S. Liu, N. El-Masry, and M. Lamvik, Appl. Phys. Lett. **75**, 1104 (1999).

[12] R. Venkatasubramanian, Phys. Rev. B **61**, 3091 (2000).

[13] G. Chen, Phys. Rev. B **57**, 14958 (1998).

[14] G. Wang and T. Cagin, Appl. Phys. Lett. **89**, 152101 (2006).

[15] T. J. Scheidemantel, C. Ambrosch-Draxl, T. Thonhauser, J. V. Badding, and J. O. Sofo, Phys. Rev. B **68**, 125210 (2003).

[16] D. I. Bilc, S. D. Mahanti, and M. G. Kanatzidis, Phys. Rev. B **74**, 125202 (2006).

[17] G. K. H. Madsen, J. Am. Chem. Soc. **128**, 12140 (2006).

[18] S. K. Mishra, S. Satpathy, and O. Jepsen, J. Phys.: Condens. Matter **9**, 461 (1997).

[19] P. Larson, S. D. Mahanti, and M. G. Kanatzidis, Phys. Rev. B **61**, 8162 (2000).

[20] S. J. Youn and A. J. Freeman, Phys. Rev. B **63**, 085112 (2001).

[21] M. Kim, A. J. Freeman, and C. B. Geller, Phys. Rev. B **72**, 035205 (2005).

[22] T. Thonhauser, T. J. Scheidemantel, J. O. Sofo, J. V. Badding, and G. D. Mahan, Phys. Rev. B **68**, 085201 (2003).

[23] G. D. Mahan, J. Appl. Phys. **65**, 1578 (1989).

[24] S. Lee and P. von Allmen, Appl. Phys. Lett. **88**, 022107 (2006).

[25] E. Wimmer, H. Krakauer, M. Weinert, and A. J. Freeman, Phys. Rev. B **24**, 864 (1981).

[26] J. P. Perdew, K. Burke, and M. Ernzerhof, Phys. Rev. Lett. **77**, 3865 (1996).

[27] http://www.flapw.de

[28] R. W. G. Wyckoff, *Crystal Structures* (Wiley, New York, 1964), Vol. 2, p. 30.

[29] H. Kohler, Phys. Status Solidi B **74**, 591 (1976).

[30] H. Kohler, Phys. Status Solidi B **73**, 95 (1976).

[31] H. Schwartz, G. Björck, and O. Beckmann, Solid State Commun. **5**, 905 (1967).

[32] A. von Middendorff, K. Dietrich, and G. Landwehr, Solid State Commun. **13**, 443 (1973).

[33] D. A. Polvani, J. F. Meng, N. V. Chandra Shekar, J. Sharp, and J. V. Badding, Chem. Mater. **13**, 2068 (2001).

[34] N. V. Chandra Shekar, D. A. Polvani, J. F. Meng, and J. V. Badding, Physica B **358**, 14 (2005).

[35] P. Larson, Phys. Rev. B **74**, 205113 (2006).

[36] R. Sehr and L. R. Testardi, J. Phys. Chem. Solids **23**, 1219 (1962).

[37] N. W. Ashcroft and N. D. Mermin, *Solid State Physics* (Harcourt Brace College Publishers, New York, 1976), p. 228.

[38] G. T. Einevoll and P. C. Hemmer, Semicond. Sci. Technol. **6**, 590 (1991).

[39] S. D. Mahanti, P. M. Larson, D. Bilc, and H. Li, in *Chemistry, Physics and Materials Science of Thermoelectric Materials: Beyond Bismuth Telluride*, edited by M. G. Kanatzidis, S. D. Mahanti, and T. P. Hogan (Kluwer Academic, New York/Plenum, New York, 2003), p. 227.